Chirp effects on impulsive vibrational spectroscopy: a multimode perspective†

Amir Wand,[a] Shimshon Kallush,[b] Ofir Shoshanim,[a] Oshrat Bismuth,[a] Ronnie Kosloff[b] and Sanford Ruhman*[a]

Received 30th September 2009, Accepted 10th December 2009
First published as an Advance Article on the web 15th January 2010
DOI: 10.1039/b920356g

The well-documented propensity of negatively-chirped pulses to enhance resonant impulsive Raman scattering has been rationalized in terms of a one pulse pump-dump sequence which "follows" the evolution of the excited molecules and dumps them back at highly displaced configurations. The aim of this study was to extend the understanding of this effect to molecules with many displaced vibrational modes in the presence of condensed surroundings. In particular, to define an optimally chirped pulse, to investigate what exactly it "follows" and to discover how this depends on the molecule under study. To this end, linear chirp effects on vibrational coherences in poly-atomics are investigated experimentally and theoretically. Chirped pump—impulsive probe experiments are reported for Sulforhodamine-B ("Kiton Red"), Betaine-30 and Oxazine-1 in ethanol solutions with <10 fs resolution. Numerical simulations, including numerous displaced modes and electronic dephasing, are conducted to reproduce experimental results. Through semi-quantitative reproduction of experimental results in all three systems we show that the effect of group velocity dispersion (GVD) on the buildup of ground state wave-packets depends on the pulse spectrum, on the displacements of vibrational modes upon excitation, on the detuning of the excitation pulses from resonance, and on electronic dephasing rates. Akin to scenarios described for frequency-domain resonance Raman, within the small-displacement regime each mode responds to excitation chirp independently and the optimal GVD is mode-specific. Highly-displaced modes entangle the dynamics of excitation in different modes, requiring a multi-dimensional description of the response. Rapid photochemistry and ultrafast electronic dephasing narrow the window of opportunity for coherent manipulations, leading to a reduced and similar optimal chirp for different modes. Finally, non-intuitive coherent aspects of chirp "following" are predicted in the small-displacement and slow-dephasing regime, which remain to be observed in experiment.

A. Introduction

Femtosecond spectroscopy provides real time coverage of chemical reactivity. Using it to construct multidimensional reaction coordinates in condensed phases, the "holy grail" of wet chemical physics, is, however, impeded by the characteristic broadening of electronic bands in solution. It erases vibronic structure and masks details of the evolving variations in bonding and geometry. Impulsive vibrational spectroscopy (IVS) can solve this by generating and later monitoring photo-induced wave packets along various nuclear coordinates during the course of a reaction.[1] By following the phase, amplitude, and frequency of the resulting spectral modulations observed with various probing schemes, structural and dynamics information regarding the early stages of photochemistry can be recorded. This approach has yet to fully realize its potential for two reasons. The first is the short pulse duration required for time resolving all active coordinates whose frequency can exceed 2000 cm^{-1}. The other is that nuclear wave packets are generated by impulsive excitation on the excited and ground electronic surfaces[2–7] and both can contribute to the spectral modulations from which dynamics are extracted (up to a dephasing time defined by the molecular system and the solvent bath). Fortunately, new pulse generation methods have been devised which routinely surmount the first of these limitations.[8,9] The latter is more persistent.

One method suggested for separation of excited and ground-state contributions to IVS signal is based on an analysis of the absolute phase of modulations which, depending on the probing mechanism, can differ for S_0 and S_1 coherences.[10–13] However, full experimental phase profiles are typically not easily interpretable and the extraction of the absolute phase of high-frequency modes is non-trivial, both limiting the applicability of this approach. The subject of this study is a complementary

[a] *Institute of Chemistry and The Farkas Center for Light-Induced Processes, The Hebrew University, Jerusalem 91904, Israel. E-mail: sandy@fh.huji.ac.il; Fax: 972-25618033*
[b] *Institute of Chemistry and The Fritz Haber Research Center for Molecular Dynamics, The Hebrew University, Jerusalem 91904, Israel*

† Electronic supplementary information (ESI) available: Optimal TL pulse for RISRS process; invariance and displacement-dependence; a note on non-degenerate oscillators; classical estimate of optimal chirp in large-Δ regime; PT analysis – detailed discussion; PT for the large-Δ regime; semi-quantitative approach to optimal chirp values. See DOI: 10.1039/b920356g

approach, employing linearly-chirped excitation pulses to make this distinction.

Chirp affects the extent of wave packet generation on the two surfaces differently due to the inherent differences in the light-matter coupling mechanisms involved.[14,15] These effects have been addressed both by theory and experiment, starting with numerical simulations of resonant impulsive stimulated Raman scattering (RISRS) excitation in model diatomics. These demonstrated that ultrafast pulses imbued with the correct amount of negative chirp (NC) could exceed their transform limited (TL) analogues in generating vibrational coherences specifically in the ground state.[14] Followed by experimental demonstration of this effect, it has been rationalized as resulting from a one pulse pump-dump sequence, with the leading blue edge serving to promote population into the excited state, only to be dumped back down by the red trailing portion. While this scenario is inherently one-dimensional, nearly all experiments have been conducted on large polyatomic chromophores in liquid solutions.

The first was published by Shank and coworkers,[16] who demonstrated IVS signal enhancements using NC pulses in an organic dye (LD690), whose spectrum is dominated by a single vibrational mode of 586 cm^{-1}. IVS modulations were enhanced by a factor of $\sim$2 for a negative chirp which broadened a $\sim$12 fs pulse in the mid visible to about 20 fs. A time-dependent perturbation theoretical analysis including electronic dephasing effects showed semi-quantitative agreement with the experimental results, also assigning a dominant contribution of the observed modulations to excited state wave packets. This stresses the difficulties in separating dynamic information on S_0 and S_1 from IVS data. Given the dominance of the 586 cm^{-1} mode, the analysis concentrated primarily on vibronic activity in that mode. More recent experiments with other laser dyes,[17] with Bacteriorhodopsin,[18] with porphyrins,[19] and with large organic chromophores[20] qualitatively verify the enhancement of RISRS with NC pulses and reiterate the inherent difficulties in separating S_0 and S_1 activity in IVS.

But even though these experiments and their simulations involve large polyatomic chromophores, interpretations have concentrated on activity of a single mode and lacked a comprehensive mapping over a broad range of pulse group velocity dispersion (GVD) conditions. Such a dense mapping has recently been reported for Oxazine-1 in methanol in a study by Malkmus *et al.*, using a non-collinear optical parametric amplifier source coupled to a flexible pulse shaper.[17] IVS modulation depths were presented for a dominant vibrational mode,[21] with comprehensive sampling of pump chirps. The functional dependence of modulation depth on GVD was retrieved, and an optimal chirp which maximizes that amplitude determined. The optimal chirp obtained for wave packet generation in the dominant 560 cm^{-1} mode was compared to predictions of a semi-classical model for a single-driven mode. Invoking the dynamical "following" of the vertical S_0–S_1 difference potential during a quarter period of harmonic motion gave an optimal chirp which matched that measured experimentally.

Despite the progress in understanding linear chirp effects on IVS, significant issues remain to be addressed. We need to know how the first and second spectral moments of the field and of the absorption spectrum influence these effects. For displaced harmonic model potentials, this translates to discovering how pump chirp effects depend on variations in ω and Δ of the active modes, and on detuning of the pump from resonance. The second moment of the field dictates the minimal pulse width, and its variation with chirp. As for the first moment, it has been shown in resonance Raman theory to affect the spectrum due to shortening of dipole coherence upon pump detuning[22]—and should have a similar effect on RISRS as well. Another issue concerns correlations between different modes in their response to excitation with chirped pulses. Even without anharmonic couplings, the electronic dipole is simultaneously modulated by all modes displaced in the electronic transition—a major issue in time-domain spectroscopic formalisms, where Franck–Condon (FC) overlaps rapidly decay in large polyatomics due to the incommensurate frequencies of the displaced modes. In analogy, excitation chirp effects on IVS could equally be mode-specific or depend on all displaced modes as well.

Aside from the fundamental significance of these questions, the potential of pulse chirp to serve as a spectroscopic tool hinges on their resolution. In the current study we address them by asking the following: the optimal chirp seems to be well-defined for a one-dimensional or quasi one-dimensional system, but what would that mean for a large polyatomic? Would the same chirp twang all active modes optimally, or would this be mode-specific? Can we refer to "dynamic following" as an explanation to this scheme, and if so—what is being followed? How would rapid electronic dephasing or tuning of the laser pulses impact the answer to the above questions? What can be learnt about the absorbing molecule from the chirp dependence of its IVS?

In order to answer these queries, IVS experiments with state-of-the-art ultrafast pulses have been analyzed by simulation of a simplified model which embodies the essence of the molecular system with a minimum of complexity. Chirped pump—dispersed TL probe experiments were conducted on ethanol solutions of Oxazine-1 (O-1), Sulforhodamine-B (S–B), and Betaine-30 (B-30), which include stable laser dyes and photo-reactive chromophores. Results show that in the small displacement limit, only the zeroth and first vibrational levels of the excited state need to be considered, emphasizing quantum mechanical aspects of the excitation process. In this limit, the effects of pump chirp are mode-specific, and follow the rules of thumb which can be expressed in terms of the vibrational frequency and the pulse GVD. The independence of different modes breaks down when large displacements are present in any vibrational mode, and both pump detuning and electronic dephasing limit the scope of chirp effects by inducing rapid loss of phase coherence into the coupled light and matter. All these effects are semi-quantitatively reproduced in matching experiments. Non-intuitive behaviour predicted for weak dephasing and low-Δ regimes remains to be observed in experiment.

B. Theory

Impulsive vibrational spectroscopy was simulated by solving the Lioville von-Neumann equation using methods previously

described.[23] The Liouville von-Neumann equation is denoted by:

$$\frac{\partial}{\partial t}\hat{\rho} = \hat{\boldsymbol{L}}(\hat{\rho}) \tag{1}$$

Here, $\hat{\boldsymbol{L}} = \hat{\boldsymbol{L}}_{\boldsymbol{H}} + \hat{\boldsymbol{L}}_{\boldsymbol{D}}$, where $\hat{\boldsymbol{L}}_{\boldsymbol{H}} = -\frac{i}{\hbar}[\hat{\boldsymbol{H}}, \hat{\rho}]$ represents the unitary part of the dynamics, and $\hat{\boldsymbol{L}}_{\boldsymbol{D}} = \hat{\boldsymbol{V}}\hat{\rho}\hat{\boldsymbol{V}}^{\dagger} - \frac{1}{2}(\hat{\boldsymbol{V}}\hat{\boldsymbol{V}}^{\dagger}\hat{\rho} + \hat{\rho}\hat{\boldsymbol{V}}\hat{\boldsymbol{V}}^{\dagger})$ is the generator of the dissipative dynamics, cast in the Lindblad form.[24] The molecule is described by two electronic states coupled by a classical electric field. The potential energy surfaces for nuclear motions are modeled by displaced harmonic oscillators. Using the rotating wave approximation in a dressed state picture, and mass-scaled coordinates, the Hamiltonian reads:

$$\hat{\boldsymbol{H}} = \begin{pmatrix} \hat{\boldsymbol{H}}_0^g & -\hat{\mu}\,\varepsilon \\ -\hat{\mu}\,\varepsilon^{\star} & \hat{\boldsymbol{H}}_0^e \end{pmatrix} \overset{\text{RWA}}{=} \begin{pmatrix} \sum_i \frac{\hat{p}_i^2}{2} + \frac{\omega_{g,i}^2 \hat{x}_i^2}{2} & -\hat{\mu}\,\bar{\varepsilon}(t) \\ -\hat{\mu}\,\bar{\varepsilon}^{*}(t) & \sum_i \frac{\hat{p}_i^2}{2} + \frac{\omega_{e,i}^2(\hat{x}_i - \Delta)^2}{2} + \hbar\delta \end{pmatrix} \tag{2}$$

where $\hat{p}$ and $\hat{x}$ represent the momentum and position operators, $\omega_{g/e}$ are the ground/excited state vibrational frequencies, $\Delta = \sqrt{\frac{\omega_e}{\hbar}}(x_{0,e} - x_{0,g})$ is the dimensionless displacement, $\hat{\mu}$ is the electronic transition dipole moment operator, and $\bar{\varepsilon}$ is the envelope of the external electromagnetic field. δ is the detuning of the central laser frequency with respect to the 0–0 transition. The electric field of linearly chirped Gaussian pulses can be written (discarding the carrier frequency):

$$\bar{\varepsilon}(t) = \tilde{\Omega}_0(\phi'')\exp\left[-\frac{2\ln 2t^2}{\tau_0^2 + 4\ln 2 i\phi''}\right] = \frac{\Omega_0}{w_F}\exp\left[-\frac{2\ln 2t^2}{\tau^2} + \frac{1}{2}i\chi t^2\right] = \frac{\Omega_0}{w_F}\exp\left[-\frac{2\ln 2t^2}{w_F^2\tau_0^2} + \frac{1}{2}i\chi t^2\right] \tag{3}$$

where τ_0 and τ are the TL and the actual temporal widths of the pulse (intensity FWHM), respectively, ϕ'' is its GVD and Ω_0 is the TL peak field. w_F is the dimensionless pulse broadening factor with respect to TL (τ/τ_0), and χ is the chirp rate (CR), *i.e.* the derivative of the instantaneous frequency: $\chi = \frac{\mathrm{d}^2\phi}{\partial t^2}$. A more thorough description of these quantities can be found elsewhere.[25]

The solvent bath is described using a Markovian dephasing model. We limit our discussion to the fastest timescale of pure dephashing described by a δ-correlated random noise, which induces the phase loss. This leads to the Lindblad form: $\hat{\boldsymbol{L}}_{\boldsymbol{D}} = -\frac{\Gamma}{2}[\hat{\boldsymbol{V}}, [\hat{\boldsymbol{V}}, \hat{\rho}]]$. Specifically, for electronic dephasing:

$$\hat{\boldsymbol{V}} = \begin{pmatrix} -\hat{\mathbf{1}}_g & 0 \\ 0 & +\hat{\mathbf{1}}_e \end{pmatrix} \tag{4}$$

where $\Gamma = \frac{1}{T_2}$ is the pure dephasing rate, and the unity operator ($\hat{\mathbf{1}}_{g/e}$) is defined over the ground/excited state subspaces. This leads to an exponential decay of the non-diagonal density matrix elements which involve two electronic surfaces (electronic dephasing only).[26] The state of the system is described by the total density operator:

$$\hat{\rho} = \begin{pmatrix} \hat{\rho}_e & \hat{\rho}_c \\ \hat{\rho}_c^{\dagger} & \hat{\rho}_g \end{pmatrix} \tag{5}$$

$\hat{\rho}_g$ and $\hat{\rho}_e$ are blocks pertaining to vibrational levels within the ground or excited electronic surfaces, respectively. $\hat{\rho}_c$ represents nuclear coherences between the two surfaces, *i.e.* vibronic coherences. All simulations assumed initial population only of the zeroth vibrational level ($T = 0$).

Throughout this paper, the pulse area $\mu\Omega_0$ is kept within the weak-field regime ($\sim 5 \times 10^{-5}$ a.u.), accounting for population transfer of less than 1% (linear excitation regime). Matrix elements of the transition dipole moment operator are given by:

$$\mu_{\vec{n}_g}^{\vec{n}_e} = \mu_{\mathrm{el}} F_{\vec{n}_g}^{\vec{n}_e} = \mu_{\mathrm{el}} \prod_m \langle \phi_{n_g^m}^g | \phi_{n_e^m}^e \rangle \tag{6}$$

where μ_{el} is the transition dipole moment (Condon approximation), and $F_{\vec{n}_g}^{\vec{n}_e} = \prod_m \langle \phi_{n_g^m}^g | \phi_{n_e^m}^e \rangle$ is the total FC factor for the transition. The amplitude of induced vibrational coherences on either surface was evaluated by the square root of the expectation value of the operator:

$$M_{g/e} = [\omega_{g/e}^2 \langle x \rangle_{g/e}^2 + \langle p \rangle_{g/e}^2]_{t \to \infty} \propto \langle \hat{a} \rangle^2 + \langle \hat{a}^{\dagger} \rangle^2 \tag{7}$$

where a and $a^{\dagger}$ are vibrational annihilation and creation operators, respectively. This measure was used for comparison with power Fourier spectra extracted from the data, and will be regarded as "modulation depth" in what follows.

In the following sections, results are reported for simulations which employ this model in a step by step approach to gain insight into the factors which govern chirp effects on IVS for poly-atomics in solution.

B.1 Single mode—excited state

Excited state wave packets are formed along displaced modes by simultaneous vertical transitions to numerous vibrational levels with non-vanishing FC factors, approximately reconstructing $|\phi_g\rangle$ on the complete basis $|\phi_e^n\rangle$ to a degree of precision which is limited only by the duration of the excitation pulse.[1] For a given pulse spectrum, a transform limited pulse should generate optimally localized excited state wave packets, and the introduction of pump chirp, regardless of sign, should diminish their amplitude.[10,16] To test this assertion, one-dimensional simulations with varying amounts of pump GVD for two values of dimensionless displacement (0.1 and 1.5) and various rates of electronic dephasing are presented in terms of the induced excited state coherences in Fig. 1.

As expected, equal amounts of negative or positive chirp reduce the amplitudes of excited state coherences similarly, with an optimal chirp of zero—*i.e.* a TL pulse. In the absence of dephasing and small displacements, a pathological conservation of coherence is obtained in the simulations, reflecting Hamiltonian dynamics with only two relevant vibrational levels contributing to the signal. This is not the case for large displacements, where numerous levels on the excited state vibrational ladder are involved; this leads to

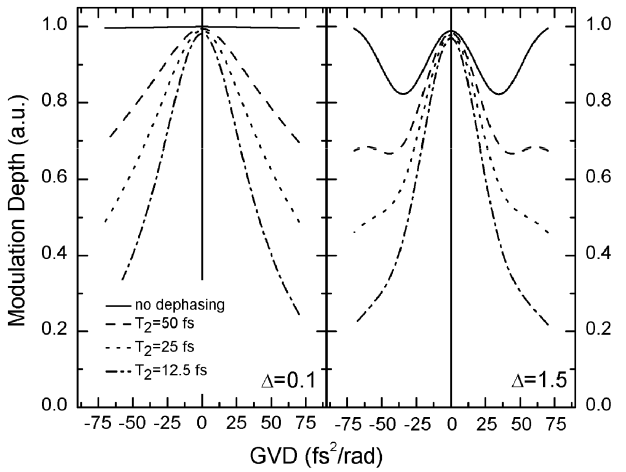

Fig. 1 Excited state modulation depth *vs.* GVD for $\bar{\nu} = 1600\ \mathrm{cm}^{-1}$, $\tau_0 = 5.6$ fs, and $\delta = 0$. Dephasing rates and displacements are designated in the figure.

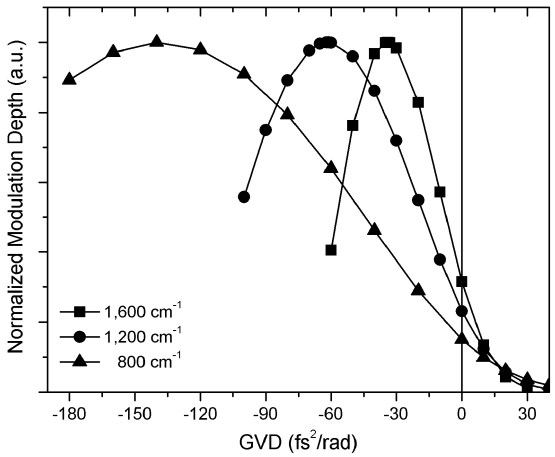

Fig. 2 Ground state modulation depth *vs.* GVD for $\tau_0 = 5.6$ fs, $\delta = 0$ and $\Delta = 0.2$ for three vibrational modes (each simulated separately as a single degenerate harmonic mode). Frequencies are designated in the legend.

revivals of coherences which are probably attributable to the harmonic approximation. For both displacements, the introduction of significant rates of dephasing results in suppression of the induced vibrational coherences upon applying chirp of either sign.

Having demonstrated the validity of these trends, the remaining simulations concentrate on ground state wave packet activity. As shown below, ground state coherence generation exhibits a richer dependence on the experimentally controlled parameters due to the inherent multi-photon nature of the underlying Raman scattering mechanism.

B.2 RISRS—single mode, no bath

Chirp effects on a pulse's ability to generate ground state coherences through the RISRS mechanism are best assessed in reference to the amplitude of modulation achieved by its TL analogue. The potential of non-chirped pulses to coherently excited ground state vibrations has been investigated and the optimal pulse duration τ_0 depends on the vibrational frequency ν as $\nu\tau_0 \cong \frac{1}{4}$ (see ESI, section A).† This duration provides sufficient evolution time on the excited state for the buildup of essential FC overlaps with many ground state levels, while conserving sufficient briefness for avoiding excessive wave packet smearing.[5,10]

Keeping this in mind, a series of RISRS simulations with varying amounts of pump GVD were conducted with the following excitation pulse parameters: $\tau_0 = 5.6$ fs, $\delta = 0$ and $\Delta < 0.5$ for a single degenerate harmonic mode. Note that according to the above relation, this is the optimal TL pulse for RISRS activation of a $\sim$1600 cm^{-1} mode. Three vibrational frequencies were tested: 800, 1200 and 1600 cm^{-1}. The results are shown in Fig. 2 as the modulation depth against pump GVD; the curves for each mode were normalized separately.

As shown in the figure, the magnitude of modulation responds very differently to addition of positive or negative chirp. Positive chirp leads to a monotonic reduction in modulation amplitudes, while shifts towards NC begin with significant enhancements up to a point beyond which a further increase leads to reduced coherence activation. This trend of improvement upon introducing NC is observed even for the 1600 cm^{-1} mode, whose modulation amplitude is enhanced by a factor of $\sim$1.5 at an optimal chirp of $\sim$–35 $\mathrm{fs}^2\ \mathrm{rad}^{-1}$. Since even the "optimal" TL pulse can be improved upon by introducing the correct negative chirp, we deduce that there is more to this effect than just "adjustment" of pulse duration to the vibrational period. The phase relations of different Fourier components of the pulse are an essential component of the story. This is also supported by the asymmetric nature of equally broadened NC and PC pulses. Moreover, for a given excitation pulse, a strong dependence exists between the optimal chirp and the vibrational frequency. As the frequency increases, the optimal NC is closer to zero GVD. This matches intuition since a faster mode requires faster "following" and accordingly a less broadened pulse. An additional qualitative analysis of the OC value is reported later. The absolute value of optimal chirp was found to correspond to a chirp rate of nearly one vibrational quantum in half a vibrational period, which describes the entire one-directional wave packet evolution (along which the vertical difference potential reduces monotonically).

The main incentive for describing intra-molecular modes as displaced harmonic oscillators is that it leads to results which are transferable between different molecules through the use of dimensionless units. In order to benefit similarly in our portrayal of the RISRS process and to minimize the number of simulations required, similar dimensionless parameters need to be identified for the excitation pulse as well. As explained in the ESI† (section B), equivalence between simulations (with respect to the optimal chirp) is achieved if all energies related with the excitation pulse, *i.e.* $1/\tau_0$, δ, as well as Γ are scaled with the vibrational frequency ν (for a given Δ). This leaves only one crucial parameter unaccounted for—the chirp or GVD. Given the time-squared dimension of GVD, a similar scaling of ϕ'' with ν^2 should lead to equivalence of single mode simulations with chirped excitation pulses as well.

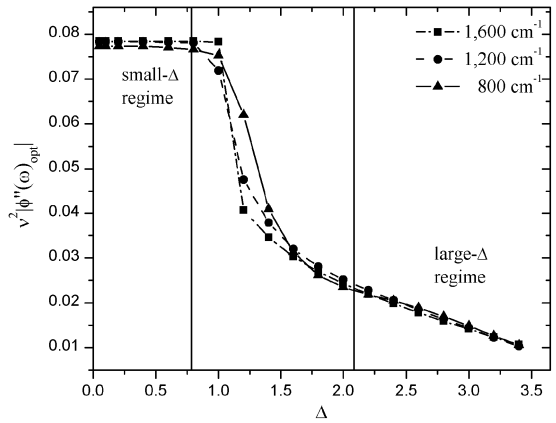

Fig. 3 Δ-dependence of modulations: optimal GVD values (scaled by ν^2) *vs.* displacement (△) for $\tau_0 = 5.6$ fs and $\delta = 0$ for the three modes presented in Fig. 2.

To test this, simulations were run for the three vibrational frequencies described above, with dense coverage of Δ and NC. For each value of Δ, an optimal chirp is determined, and plotted after the correct scaling (against Δ). As demonstrated in Fig. 3, rescaling ϕ'' by ν^2 leads the curves obtained for all three frequencies to coincide. These curves also demonstrate that for a given vibrational frequency, the chirp dependence breaks displacements into 3 effective ranges. From zero to ~0.75 (small Δ regime) the optimal chirp is Δ-independent and relatively high. From $\Delta \sim 0.75$ to ~2, a precipitous fall occurs in optimal negative chirps, while in the high-Δ regime, above this, only gradual further reduction in optimal chirp is apparent.

The trends observed for low and high values of Δ can be explained as follows. For very low displacements, Franck-Condon factors fall off sharply with $\Delta\nu = \nu'' - \nu'$. Thus, as far as the RISRS process is concerned, only two vibronic transitions matter: 1″–0′ and 1″–1′, leading from the zeroth and first vibrational level in S_1 to $\nu = 1$ in S_0. These two transitions are separated in energy by a single vibrational quantum which the chirp must cover in a period which scales as $1/\nu$. Since these considerations will not change with further reduction of Δ, the optimal chirp should reach an asymptotic level as is in fact observed. Furthermore, since the chirp rate is nearly proportional to $1/\phi''$, the optimal GVD should scale as $\sim 1/\nu^2$, again in agreement with the simulations. A similar reasoning was found to be adequate also to non-degenrate oscillators, as shown in the ESI† (section C). Thus, the low−Δ regime is quantum in nature, involving a sparse set of relevant states and a vibrational degree of freedom which is well-represented as a two level system for each electronic surface. The high value of optimal chirp in this range reflects the relatively small energy span which the chirp needs to cover to "follow" the evolution.

The picture changes once the electronic transition induces large vibrational displacements. The range of potential energy difference swept out by the excited molecules is larger in this range and Δ-dependent. In fact, it may even exceed the frequency spread of the excitation pulse itself. All these considerations predict that the optimal chirp will be much smaller, so the chirp rate can match the rapid changes taking place in the potential gap and retain resonance. This regime is semi-classical in nature with changes in energy much larger than a single vibrational quantum, excitation to many vibrational levels on both surfaces, and wave packet dynamics which closely resemble the motion of a classical particle (see section D in the ESI).†

Having investigated how chirp effects vary with Δ, a comment on typical values of this measure in real molecules is appropriate. In large organic chromophores, transitions to bound non-reactive electronic states rarely involve displacements which extend beyond $\Delta = 1$ in reduced units. Accordingly, in most laser dyes almost all vibrational modes are in the small displacement regime. This is not the case for photochemically reactive species, where a reaction coordinate, often corresponding to low-frequency torsions in the excited state, translate into very large displacements in those modes when modeled as displaced harmonic oscillators.

B.3. Perturbative analysis

In order to uncover the quantum interference processes which underlie the effects of pulse chirp on RISRS excitation, particularly in the low displacement regime, a perturbative description of ground state IVS was constructed. To second order in the field, ground state coherences are formed as a sum over all paths in the Feynman diagram, some of which are depicted in Fig. 4. They build up the off-diagonal matrix element $\rho_g^{1,0}$, which in lieu of bath interactions is directly proportional to $|1\rangle_g$:

$$|1\rangle_g(t) = -\tfrac{i}{\hbar}\mu \sum_n F_1^n \int_{-\infty}^{t} \varepsilon^*(t')|n\rangle_e(t') \exp(-\frac{i}{\hbar}E_1^g(t-t'))\,\mathrm{d}t' \equiv \sum_n \tilde{P}_n(t) \tag{8}$$

where $|n\rangle_e$ is given by 1st order PT:

$$|n\rangle_e(t) = -\tfrac{i}{\hbar}\mu F_0^n \int_{-\infty}^{t} \varepsilon(t') \exp(-\frac{i}{\hbar}E_n^e(t-t'))|0\rangle_g\,\mathrm{d}t' \tag{9}$$

Here $F_n^m = \langle\phi_n^g|\phi_m^e\rangle$ represent the FC factors, and $\tilde{P}_n$ is the amplitude of the Feynman path that goes through the level n in the vibrational ladder in the electronic excited state (see section E in the ESI for details).† The displacement proportionality of the FC-factors that couple the states is denoted in Fig. 4.

As stated above, for small values of Δ, only two paths—P_0 ($0_g \rightarrow 0_e \rightarrow 1_g$) and P_1 ($0_g \rightarrow 1_e \rightarrow 1_g$)—have significant FC factors. The amplitudes and relative phases of these two paths are plotted in Fig. 5 *vs.* pump GVD for $\bar{\nu} = 1600$ cm^{-1}, $\tau_0 = 4.3$ fs, and $\delta = 0$ in the left and right panels, respectively. The mode was kept within the small-displacement regime ($\Delta < 0.5$). Note that the amplitudes of both paths for each GVD are similar, so that these curves overlap in the figure.

Moving from TL to NC pulses, the amplitude of both paths increases, up to a point where it reaches a plateau (at about -30 fs^2 rad^{-1}). The phases of both paths start at opposite signs (due to inversion of signs of FC factors), and as GVD is

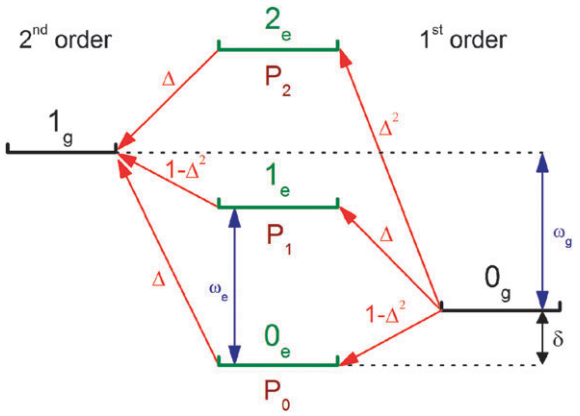

Fig. 4 A partial Feynman diagram of RISRS excitation for one vibrational mode, including three paths (P_0, P_1 and P_2) leading from $|0\rangle_g$ to $|1\rangle_g$. Arrows denote the significant first and second order transitions, with their corresponding Franck–Condon intensities. δ denotes pulse detuning from resonance.

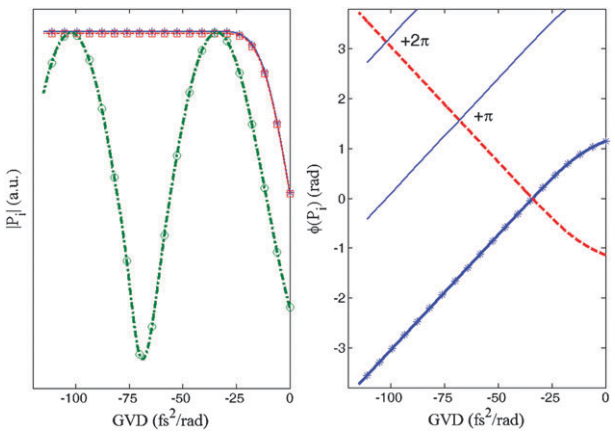

Fig. 5 Contributing paths to RISRS coherences. (left) Absolute values of P_0 and P_1 are presented in solid and dashed lines, respectively (overlapping lines). The dotted-dashed line represents the absolute value of $P_0 + P_1$. (right) Phases of both paths. Thin lines refer to the phase of P_0 shifted by integer multiples of π.

increased, change linearly in opposite directions. A similar result has been observed for a three-level atomic system.[27] Results show clearly that the optimal chirp is that for which the interference between the two paths, P_0 and P_1, is constructive: phase(P_0) = phase(P_1) $\pm$ $2n\pi$. This is akin to many coherent control scenarios, where interference between two quantum paths is used to optimize population of a desired quantum state.[28] Thus, in the low-Δ regime, chirp effects on RISRS excitation can be cast in the language of coherent control. This portrayal also explains the revivals observed for GVD's beyond the first maximum in the modulation depth, shown in the figure. Since only 2 channels are active in the buildup of ground state coherence, the chirp which leads to constructive interference will induce the same modulations, regardless of the resulting pulse duration. This counter-intuitive phenomenon is opposed to traditional explanations of the IVS, based on the fact that the pulse duration is less than a single vibrational oscillation period.[1] Such revivals of RISRS activation at higher GVD values have not been reported, probably due to effects of dephasing which are not included here (see below). As Δ increases, other paths contribute, making a perturbative approach less transparent, but the same reasoning applies (see section F in the ESI).†

For positive GVD values, the absolute contributions of each of the paths decrease to zero and the total modulation vanishes. This can be explained by the reduction near GVD = 0 of the absolute amplitudes of both channels—both requiring a "blue" interaction to precede a "red" one. Classically, this reduction directly reflects the transition to a pulse chirp which causes the Fourier components to arrive in the opposite order, red *before* blue. Naturally this will extinguish two photon interactions which require the opposite ordering, and no combination of phases can remedy this as observed. See additional discussion in section G of the ESI.†

B.4 Detuning

Another pulse parameter whose effect on the RISRS process must be assessed involves δ, the detuning of the pulse's first spectral moment from the 0–0 transition frequency. Fig. 6 presents the modulation depth *vs.* GVD for three different values of blue detuning of the excitation pulse with regard to the 0–0 transition for a low-displaced 1600 cm^{-1} mode, along with the curve for the zero-detuning case. Investigation of red shifts for this model also shows that it affects modulation depth identically to a blue detuning of equal magnitude (within the small-Δ regime). The solid, dashed, dotted and dotted-dashed lines refer to detuning of δ = 0, 1.0ν, 2.5ν and 4.0ν. As the detuning is enlarged, the modulation depth decreases noticeably and the optimal chirp is shifted towards smaller GVD absolute values. Moreover, an effect of "flattening" the dependence for asymptotic values is evident. This is a result of the increase of δ which tunes P_0 out of resonance and decreases its amplitude for large GVD's, causing the total modulation to be less chirp-sensitive. It also relies on the lack of electronic dephasing (bath effects) in these simulations (which causes a decay of the coherences for large GVD values; see next subsection).

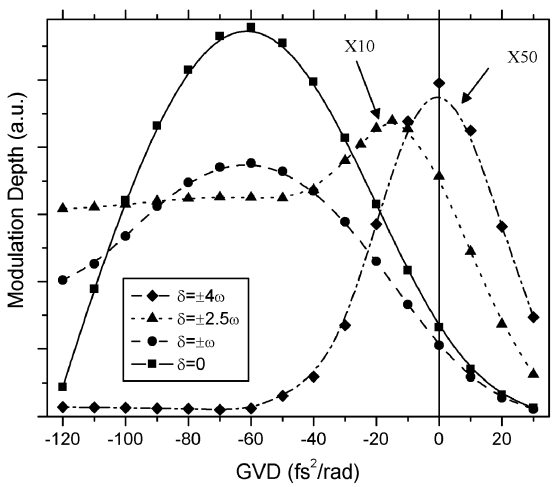

Fig. 6 Detuning effects: modulation depth *vs.* GVD for an oscillator frequency of 1600 cm^{-1} and four detunings which are designated in the figure. Curves for large δ's were rescaled as denoted.

B.5 Electronic dephasing

In order to add bath effects to the simulations, electronic dephasing was included according to eqn (4), while vibrational dephasing was neglected due to its irrelevance on the short excitation timescales. Fig. 7 presents the total modulation depth *vs.* GVD for five different dephasing rates (corresponding to T_2 of 500, 50, 25, 12.5 and 5 fs) for a low-displaced ($\Delta = 0.1$) 1600 cm^{-1} mode and for $\tau_0 = 4.3$ fs (same parameters used before in Fig. 5 and 6), along with the contributions of the individual Feynman paths to the total modulation in this case. Single path contribution was computed separately by eliminating the second channel, and the relative phase was defined by comparison of amplitudes obtained in single-channel simulations and the total resulting amplitude. The main frame presents the total modulation *vs.* GVD, where different lines refer to different pure dephasing times (T_2), as denoted. The upper panels present the magnitude and relative phase of both paths. The electronic dephasing leads to an exponential decay of the magnitude of paths as a function of the GVD, which leads to a decay in the total modulation. However, the relative phase between adjacent paths is barely influenced by the dephasing.

As expected, the electronic dephasing—which narrows the window of opportunity for coherent manipulations—shifts the optimal chirp to lower values. The effect is prominent for lower frequencies, which are more vulnerable to the shortening

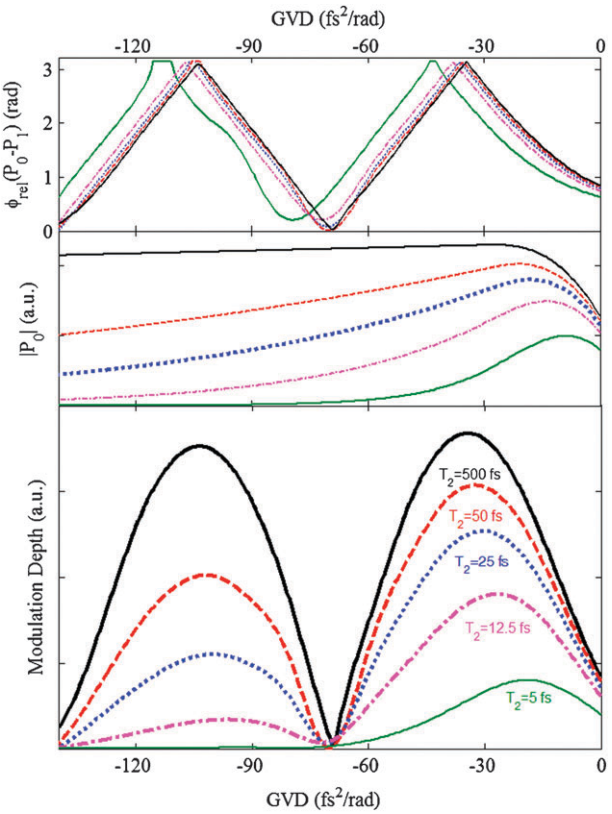

Fig. 7 Electronic dephasing effects: modulation depth *vs.* GVD with electronic dephasing for a vibrational frequency of $\bar{\nu} = 1600$ cm^{-1}, and $\tau_0 = 4.3$ fs, $\Delta = 0.1$ and $\delta = 0$ (lower panel). Middle and upper panels present $|P_0|$ ($=|P_1|$) and relative phase of P_0–P_1, respectively. Dephasing rates are denoted in the lower panel next to the curves.

of the transition dipole lifetime. Thus, the optimal chirps of different modes in the presence of fast dephasing are similar, especially when considering experimental errors. Revival feature survives until its extinction for $T_2 < 12.5$ fs, suggesting that in this respect it might be observed experimentally even in condensed phase. Moreover, as these revivals are observed for the low-Δ regime, where only two levels are involved in the generation of RISRS signal, it seems that they are not the result of the harmonic approximation.

Similar bath effects on chirped excitation were reported also for very different control scenarios, such as the achievement of electronic population inversion using PC pulses when T_2 becomes comparable to or even smaller than the pulse duration.[29]

B.6 Multiple modes

The generalization of the 1-D scenario to multiple modes poses the question of correlations between the dynamics of different active degrees of freedom. To investigate this, our simulations were extended to include two modes (see section E in the ESI).† In this case, a path is denoted by two subscripts (i and j): P_{ij}, where each subscript refers to one of the normal modes (x or y) based on our previous formulation. Fig. 8 exhibits chirped pulse RISRS simulations for an isolated molecule with two degrees of freedom, one slightly displaced (1200 cm^{-1}), and another of varying displacement (1600 cm^{-1}).

Clearly, as long as both modes are in the small displacement regime, their response to variations in GVD is independent and mode-specific. This situation changes once one of the modes exceeds this limit. The variation over time of the FC overlap in the highly-displaced mode strongly modulates the amplitude of the transition dipole which depends on all single mode overlap integrals. This transition dipole is the handle by which the field continues to alter the material state throughout the chirped excitation, and the loss of its coherence due to the temporary decay of overlap impairs the ability of continued manipulation in all vibrational modes. This is particularly true when the largely displaced vibration is of high frequency since its decay of overlap will be all the more rapid, and interfere with dynamics of other dependent modes more effectively. This Δ-dependent correlation between the light driven dynamics in different modes has a close analogy with multi-mode dynamic dephasing effects in resonance Raman spectroscopy. The radiating dipole which gives rise to the Raman scattering is limited in lifetime by the dynamics in all active modes, but mostly by those which are highly displaced for precisely the same reasons.[30] In both cases, those modes dominate and control the extent of the dynamics which is recorded by the spectroscopy.

Cast in Feynman paths terms, the source of correlations is clear, as seen in the inset of the figure. Enlargement of the displacement of the first mode induces a trivial result on the mode itself (enhancement of FC factors of higher paths), without significant contribution from paths involving the second mode. But, the second mode is built of significant contributions of paths resulting from excitation of the first mode, breaking the orthogonal nature of excitation of multiple-modes in the low-Δ regime.

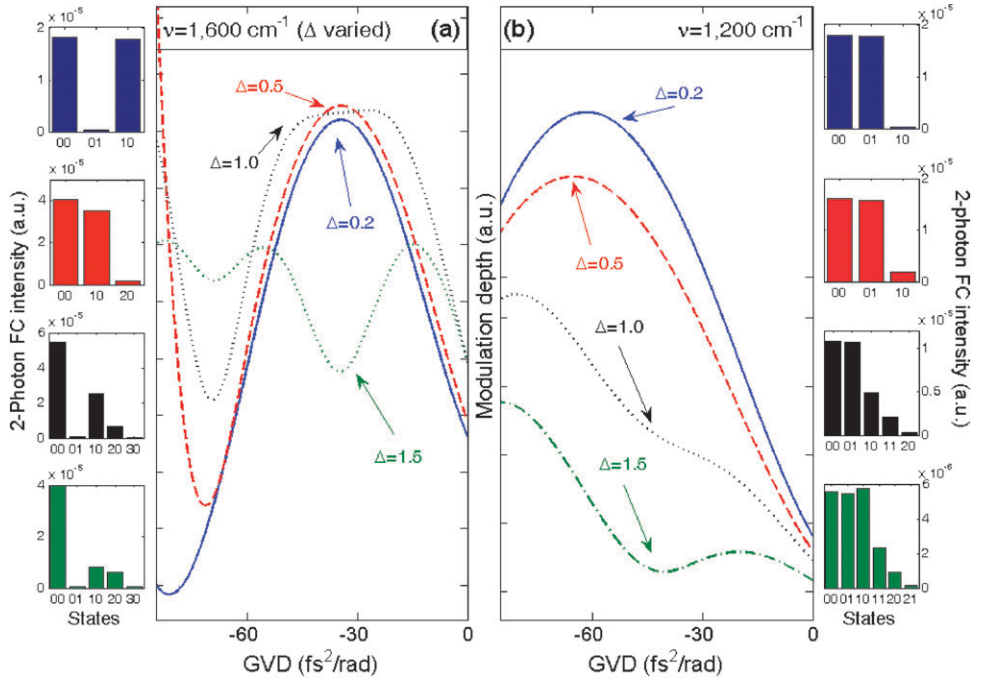

Fig. 8 Modes correlations: (main panels) the modulation depth of the two modes ($\bar{\nu}_x$ = 1600 cm^{-1}—left panel, $\bar{\nu}_y$ = 1200 cm^{-1}—right panel) is plotted *vs*. GVD for a variety of displacements of the fast mode, while the slow mode is kept within the low-Δ regime (the Δ's denoted refer to the fast mode in both panels). (insets) significant two-photon FC intensities for ascending values of Δ for each mode using the corresponding same color coding. The indices of the paths for this two-dimensional case are described in the text.

C. Experimental method

Betaine-30 (Aldrich), Oxazine-1 (Radiant Dyes) and Sulforhodamine-B (Exciton) were dissolved in Ethanol (spectroscopic grade, Merck) and peristaltically pumped through a 0.25 mm path length flow cell equipped with 120 μm quartz windows, at a rate which replenished the sample between shots. Solution concentrations were adjusted to obtain optical densities of ~0.4 at the absorption peaks. The light source was a home-built multipass amplified Ti:Sapphire system described in details elsewhere,[18,31] and operated at a repetition rate of 400 Hz. Its output consisted of ~30 fs pulses centered at 790 nm, contatining 0.6 mJ of energy. 50% of the amplifier output pumped a commercial non-collinear parametric amplifier (NOPA plus, Clark-MXR) which was reconfigured to a single amplification stage of 2 mm BBO, producing 3 μJ pulses with a spectral width of 100 nm FWHM.

NOPA intensity spectra used in the experiments are shown in Fig. 9, along with steady state absorptions of the dye solutions. NOPA-I pulses were used for B-30 and O-1 samples, while NOPA-II (red-shifted with respect to NOPA-I) were used for S–B. The pulses were pre-compressed in BK7 prisms, and passed into a zero dispersion shaper, constructed from a 600 mm^{-1} grating, a silver-coated 30 cm focal length spherical reflector and a 19 channel aluminium coated deformable mirror (DM, OKO Flexible Optical).[32] Compression was achieved by maximizing second harmonic generation (SHG) in a 20-μm BBO crystal, using an automated random searching routine based on a genetic algorithm.[33,34] Compression was verified by pump–probe cross-correlation measurements and X-PG-FROG using amplifier fundamental pulses and a fused silica cover slip as Kerr gate.[35]

The NOPA pulses were split into pump, probe and reference beams using fused silica metallic beam splitters, which were compensated for in the appropriate beam paths. The shaper was used only to optimally compress the pulses to the TL of about ~6 fs. The probe pulses were maintained at TL, while pump pulses were linearly chirped by insertion or removal of differing amounts of fused silica in the pump beam path, covering a GVD range of ±150 fs^2 rad^{-1} as verified using X-PG-FROG. The pump (~150 nJ pulse^{-1}) and probe beams were focused to a $1/e$ intensity diameter of 120 μm using reflective optics. The data were demonstrated to be linear in pump and probe intensities to at least twice the fluence used in

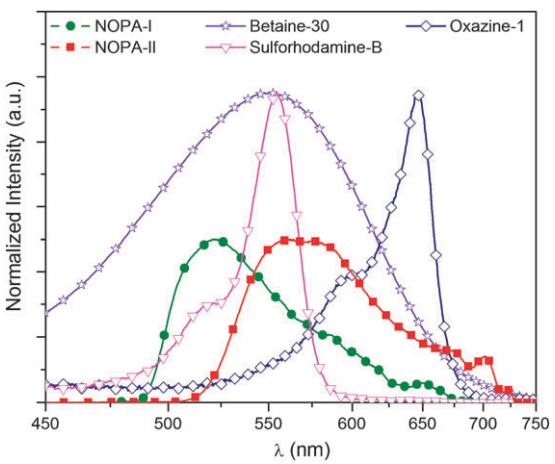

Fig. 9 Steady state absorption spectra of B-30, O-1 and S–B in ethanol, along with NOPA pulse spectra employed: NOPA-I for B-30 and O-1 and NOPA-II for S–B (see text for details).

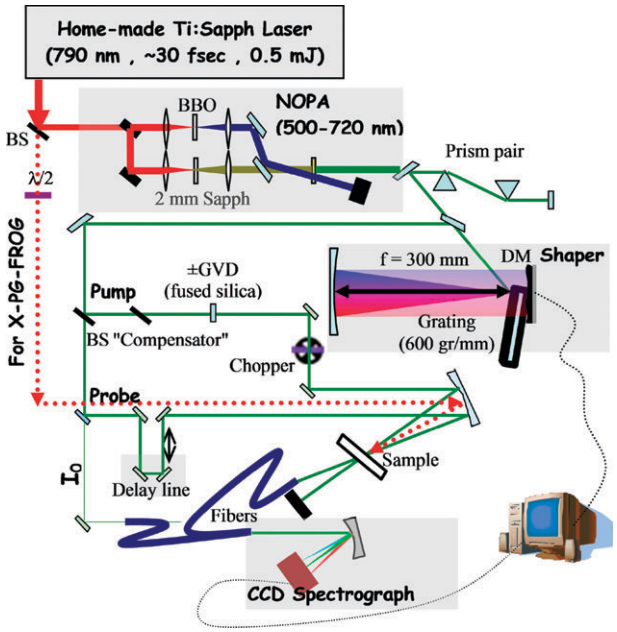

Fig. 10 Experimental setup (see text for details).

the reported experiments. Transmitted probe and reference (I_0) pulses were co-dispersed in a 1/8 meter imaging CCD spectrograph (Oriel/Andor) to obtain delay-dependent ΔOD spectra from ~500–700 nm. A sketch of the system is presented in Fig. 10.

D. Experimental results

D.1 Primary results and analysis procedure

Sulforhodamine-B (S–B), Oxazine-1 (O-1) and Betaine-30 (B-30) were chosen since all contain active vibrtaional modes over a broad range of frequencies, while representing very different cases of photoreactivity and detuning. Unlike O-1 and S–B, B-30 undergoes ultrafast solvation and photochemistry which are reflected in its extensive solvent-dependent spectral broadening and solvatochromism. O-1 is very similar to S–B in spectral broadening and photostability, but is very different in its detuning from the NOPA pulse spectrum (Fig. 9).

Chirped pump—hyperspectral probe experiments were conducted for these three dyes. Raw data consist of ΔOD matrices at different probe wavelength and time delays. Panel (A) of Fig. 11 presents a color-coded contour map of such data for S–B in ethanol.

Periodic modulations are discernible as vertical ripples in the color map—readily observed in horizontal cuts, such as that presented in panel (B) for λ_{probe} = 530 nm. Modulations were isolated by subtraction of a slowly varying background, and the residuals (see inset of panel (B)) were Fourier analyzed as shown in panel (D) for the same wavelength. The Fourier power spectrum exhibits well-defined peaks which correspond to normal modes of the solute along with those of the solvent. Panel (C) presents the full power DFT contour map for the same data of panel (A), demonstrating the probe-wavelength dependence of the DFT signal, not accounted for in our simulations. The dominant solvent mode (around 884 cm^{-1}) is not shown. As previously described, the amplitude of absorption modulation is maximal on the wings of the absorption band, goes through a minimum near the peak, resembling the derivative of the absorption band,[6,17,18] and reverse phase on either side of that central minimum as described later.[5,12,13,36] Moreover, as the vibrational frequency increases, so does the spectral breadth of oscillatory activity, particularly to the red of the absorption peak.[10] This is in analogy with the larger contribution made by high frequency modes to the breadth of molecular absorption spectra.[18]

The peaks observed in the Fourier spectra of all three dyes were compared with known ground state vibrational frequencies where available,[37,39] and found to be identical within experimental error. DFT power spectra obtained from residuals at $t > 80$ fs at different pump chirps are presented in Fig. 12 for S–B for a probe spectral window of ~20 nm centered at 530 nm, which is on the blue wing of the absorption peak presenting high S/N ratio in the modulations (similar considerations were taken in choosing probe wavelength for analysis in the other dyes, presented next). The chirp effects on solute mode modulations qualitatively agree with expectations based on the RISRS simulation results. While all features are attenuated for positive pump chirp, significant enhancements are evident for negative GVD. This trend continues further for lower frequency modes as expected. In contrast, the solvent mode (denoted by asterisks) is diminished for all chirps, as expected for off-resonance ISRS.[12]

These trends are presented in Fig. 13 which plots integrated peak areas *vs.* pump GVD for various normal modes. The asymmetry between PC and NC is obvious, the former suppressing coherence in all active modes, to a degree that monotonically increases with the increase of chirp. In contrast, small NC enhances the RISRS signal of all modes. The dense sampling of GVD allows for a definition of the optimal chirp for obtaining a maximum in depth of modulation. The optimal chirp is mode-specific, peaking at smaller GVD values the higher the mode frequency, as predicted by model simulations above. In this respect, both O-1 and B-30 exhibit behavior different than that of S–B. Coherences in the former two are maximized by a lower and nearly identical optimal chirp for all modes studied. The steepness of the fall-off above and below the optimal chirp is, however, mode-specific and an asymmetry in the rate of amplitude fall-off with GVD for NC and PC is also observed (see Fig. 16 and following discussion).

D.2 Modulation phase and amplitude profiles

Absolute phase retrieval is a unique IVS feature which can aid in identifying the electronic surfaces involved in a specific component of spectral modulation.[2,5,12,36,38] The Fourier mapping obtained from the S–B data was therefore analyzed to provide absolute modulation phases for the prominent bands assuming $R(t;\lambda) = \sum_n A_n(\lambda)e^{-t/\tau_n}\cos(\omega_n t + \varphi_n(\lambda))$, where R is the λ-dependent residual, and φ_n is the absolute phase of a contributing Fourier component. Accordingly, integer values of phase indicate ±cosine like behavior, while half integers represent ±sine dependence. To obtain this

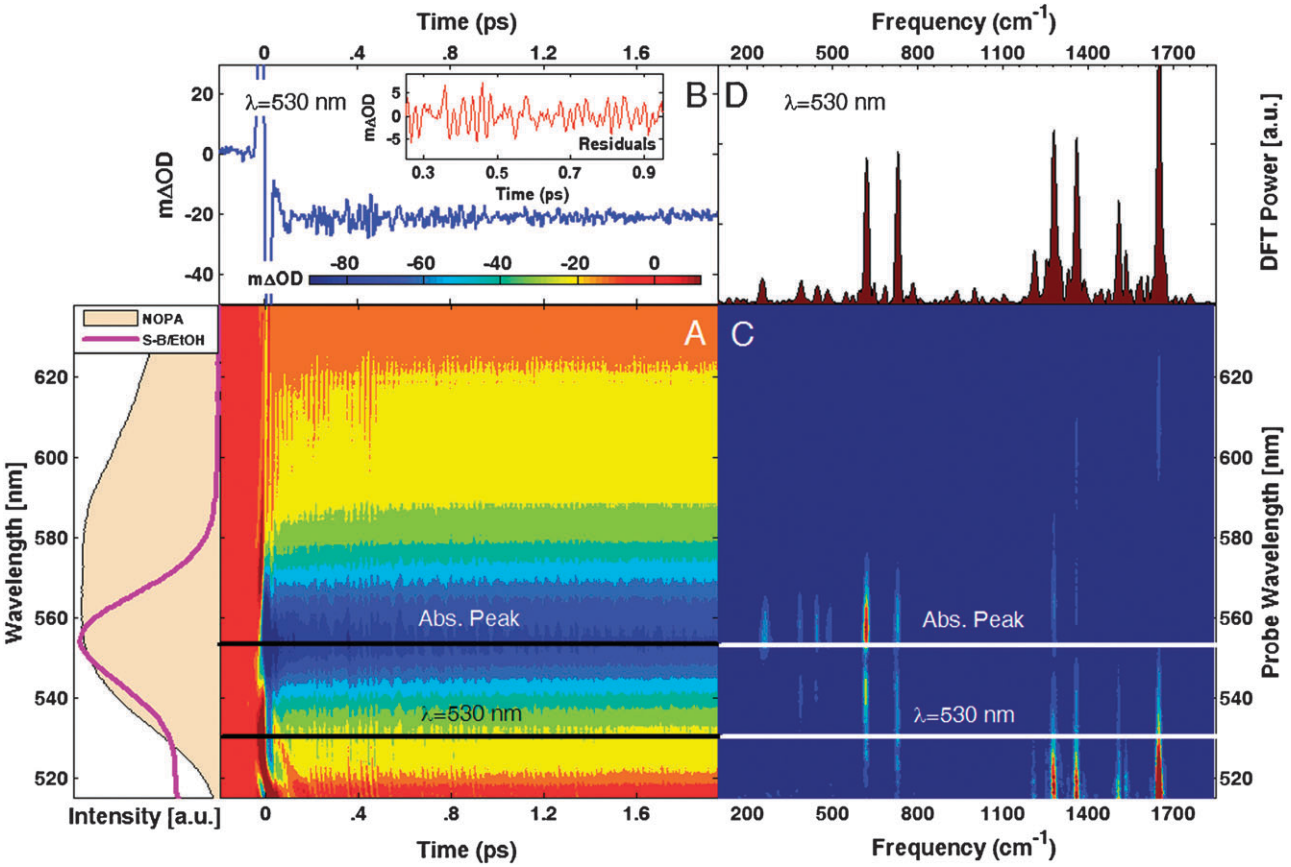

Fig. 11 Sulforhodamine-B data analysis. Panel (A) presents a color-coded contour map of the raw data (ΔOD), and panel (B) a cut of the transient absorption along a given probe wavelength (residuals obtained by a subtraction of a slow varying function are shown in the inset). Panels (C) and (D) present the same data in the frequency domain (DFT, intensity) for all wavelengths and for a given cut, respectively.

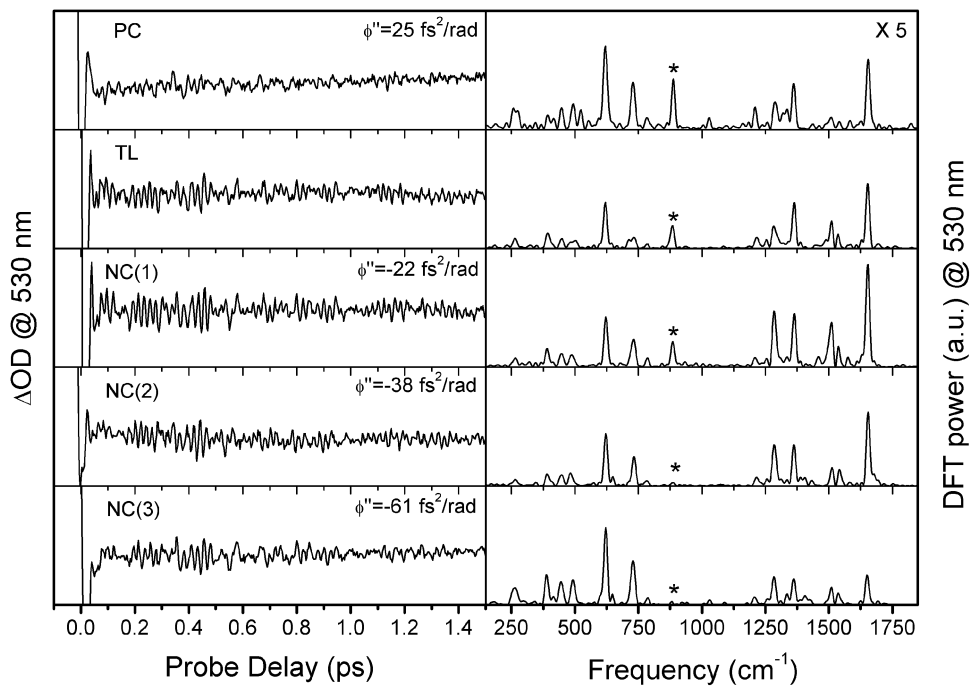

Fig. 12 ΔOD (left) and DFT power (right) *vs.* GVD for S–B and a probing wavelength window of 530 ± 10 nm. DFT maps were extracted as described in the text. The mode ~884 cm^{-1} (signed by an asterisk) is assigned to the solvent (ethanol).

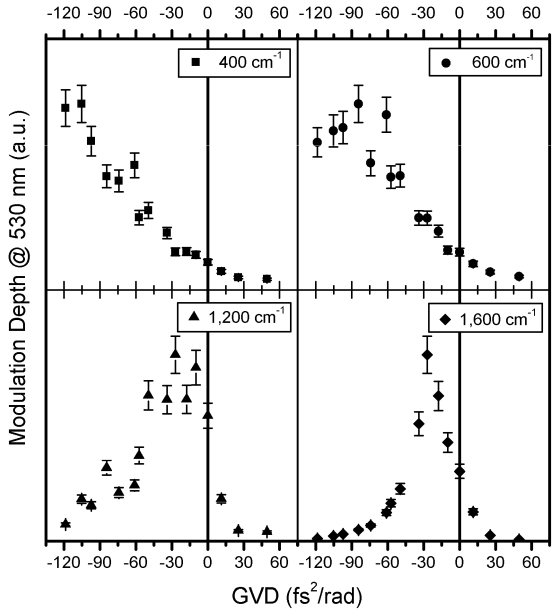

Fig. 13 DFT power *vs.* pump GVD for four different vibrational modes of S–B, extracted from the same probing window as the data in Fig. 12.

mapping, phase was extracted directly from the residual matrix using $\varphi = \arctan(\mathrm{Im}(FT\{\mathrm{res}\})/\mathrm{Re}(FT\{\mathrm{res}\}))$, after determining the zero of pump–probe delay with high precision. To overcome the routine definition of inverse tangent phase ($-\frac{\pi}{2} \leq \varphi \leq \frac{\pi}{2}$), a phase retrieval based on all four quadrants was used (arctan2). Based on reproducibility of phase values from repeated measurements, the error in phase is estimated to vary from $\pi/10$ to $\pi/4$, depending on the mode frequency.

Fig. 14 presents the resulting phase/intensity mapping for two S–B modes along with one due to the solvent in the same experiment. The latter, as expected, exhibits significant amplitude wherever the first derivative of the probe spectrum is substantial, and a π-phase jump between integer values (cosine behavior) near λ_{max} of the probe. These characteristics are consistent with off-resonance impulsive excitation resulting in a pure momentum kick to the transparent ethanol vibrations.[2] The ensuing dynamics are later read out through the resulting periodic spectral shifts induced in the probe spectrum. Solute vibrations behave differently and exhibit alternative wavelength dependence both in phase and amplitude. Appreciable intensities are observed primarily around the S–B absorption peak, which is slightly shifted with respect to the NOPA spectrum, with a pronounced minimum slightly red shifted from λ_{max}. The double-humped intensity contour described above is more spread out in the high frequency mode, which also displays a more gradual phase variation with probe wavelength. A similar trend was accounted for in the works of Kumar *et al.* where temperature—rather than frequency—was varied,[12] and recently observed by Luer *et al.* in carbon nanotubes[36] and by Braun *et al.* in O-1 in methanol.[17] The low-frequency modes, whose extracted absolute phase is more reliable, tend asymptotically to half integer phase limits (sine behavior), with a π-jump near the mid point of both intensity maxima,[13] both of which are in accordance to RISRS known features.

The phase mapping in Fig. 14, as those extracted by others,[17,35] were obtained with TL pump pulses, and are clearly more complex than a simple π-jump, due to an interplay of dispersion and absorption. In order to check the possibility of joint IVS contributions from excited and ground state electronic surfaces, phase profiles were extracted for different pump chirps as shown in Fig. 15. Negligible variations in phase maps accompany the changes in pump GVD, and vertical translation of the curves is necessary to avoid their overlap. This invariance in the phase contour is obtained to within a constant phase shift, as the origin of pump–probe delay is not simple to determine in the presence of significant chirp. The only discernable variations are for the low-frequency mode at red probe frequencies where the rapid rise

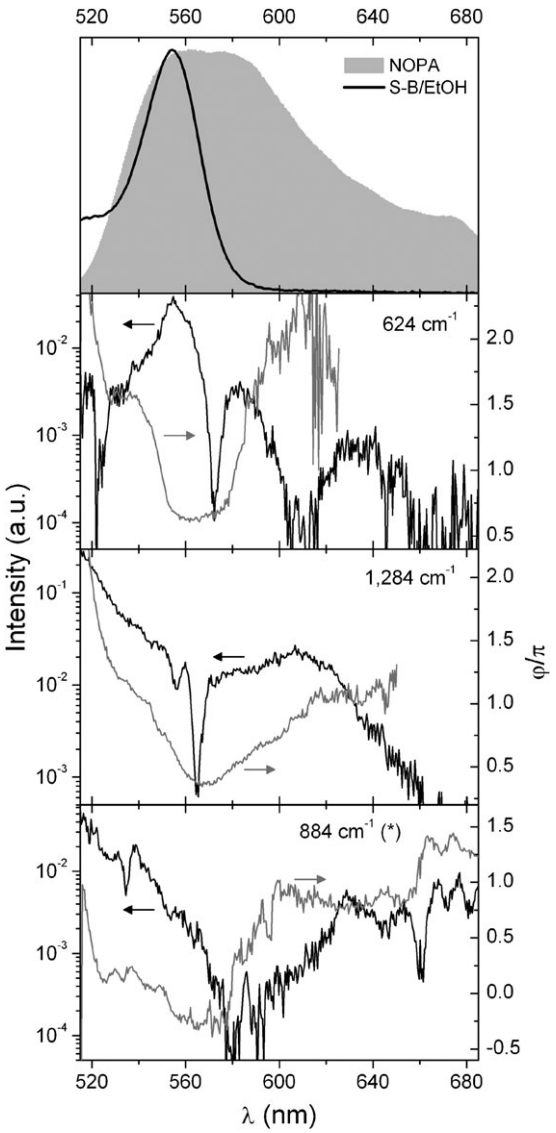

Fig. 14 Phase (gray lines, right axis, shown as multiples of π) and intensity (black lines, left axis, shown on a logarithmic scale) of modulations *vs.* dispersed probe wavelength for two different vibrational modes of S–B in ethanol (two upper panels), along with the solvent's dominant mode (lower panel).

in phase apparent with PC is smoothed out and diminished when subjected to NC pulses.

This is opposed to a previous report regarding LD690 by Bardeen *et al.*,[16] who observed different phase-jumps for NC pulses comparing to TL and PC pulses; these were interpreted as an increased contribution of ground-state coherences in the NC case. In our case, the strong asymmetric chirp dependence of the modulation intensities, along with the invariance of the phase profiles to chirp, must reflect a dominant IVS contribution from the ground state coherence.

D.3 Comparison with theory

After data from the other dyes were equivalently analyzed, modulation depths for all three *vs.* GVD are shown for selected modes as markers in Fig. 16. The solid lines represent best-fit simulations, to be described next.

Unlike the trends in S–B, O-1 and B-30 exhibit a nearly identical optimal chirp for all modes. The steepness of the fall-off above and below the obviously negative optimal chirp is, however, mode-specific, slower the lower the mode frequency is. To appreciate the reason for these differences, simulations were conducted using the described model. The dyes studied present different admixtures of the factors which influence chirp effects on IVS, and those factors need to be assessed before the relevant parameters can be derived for reproducing the experimental trends.

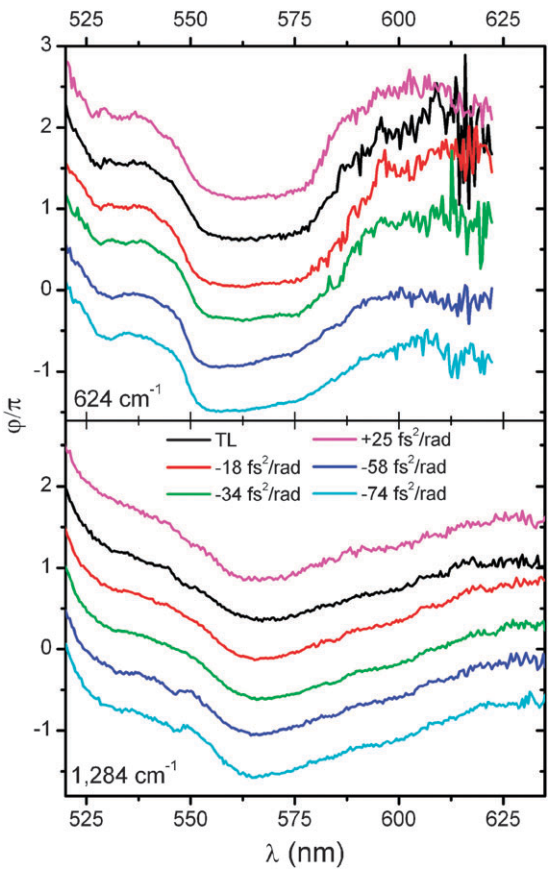

Fig. 15 Phase variation *vs.* dispersed probe wavelength for the same solute modes presented in Fig. 14 for different values of pump GVD. Curves corresponding to chirped excitation were vertically translated to avoid overlapping.

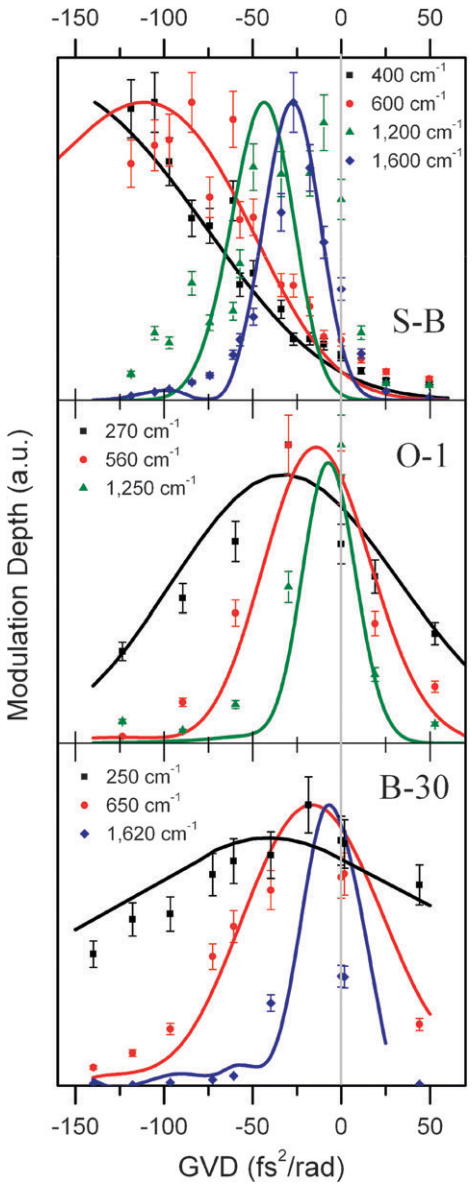

Fig. 16 DFT power *vs.* pump GVD for various modes in all three dyes. Data points are compared with best fitting simulation curves (see text for details).

The structured and asymmetric spectra of S–B and O-1 demonstrate that they are models for a small-Δ regime with moderate rates of dephasing.[37] They differ, however, in the degree of detuning between the laser pulse and the apparent transition peak, with the former near resonance, and the latter significantly blue detuned (see Fig. 9). This enables probing the detuning effects on the chirp-dependence in isolation. Since no explicit allowances are made in the simulations for dynamic solvation, detuning relates to the 0-0 transition in the liquid, and not to that in isolated molecules. B-30 presents a very different admixture, with fast excited state electron transfer reflected in its smooth structure-less absorption spectrum.[38] The transition is dominated by highly-displaced low frequency modes[39,40] which induce very rapid reactive dephasing.[41]

Following the qualitative trends outlined above, simulations with fine adjustments to the parameters were conducted to reproduce the chirp dependence of modulation depths in all three dyes. S–B and O-1 active modes were accordingly simulated with a single mode. In the former, the only variable parameter used to obtain agreement with the experimental normalized chirp dependences was Γ, the electronic dephasing rate. In view of the similar appearance of both absorption spectra, the same Γ was used for O-1 also, subject to an additional blue detuning of the excitation pulse by 3600 cm^{-1} with results shown in Fig. 16. The electronic T_2 which produced these fits was only 12.5 fs, but allowed satisfactory fitting of the chirp profiles for modes ranging from 300 to 1500 cm^{-1} in both chromophores.

Elaborate published models of medium effects on B-30 spectroscopy are clearly overkill for the semi-quantitative reconstruction aimed at here.[39] Thus to represent both rapid inertial solvent response as well as reactive intramolecular motions, chirp effects on the remaining bound chromophore modes were simulated in the presence of a highly-displaced low-frequency mode $\{\bar{\nu} = 280\ cm^{-1}, \Delta = 8\}$,[42] and a detuning of 2500 cm^{-1}. Results for two of these normal modes (Δ's for which were taken from RR studies[39]) along with the "reactive" coordinate are depicted in the lower panel of Fig. 16. A nearly perfect agreement within the experimental uncertainty was achieved again, with these physically reasonable parameters and larger deviations for the slow "reactive" mode.

E. Discussion

In view of the good agreement between simulation and experiment, it is tempting to test whether the fitting process has also led to physically meaningful parameters. We do this by comparing them with similar measures extracted by other means for these or closely related systems. In lieu of literature values for electronic T_2 of S–B in ethanol, comparison is made with parameters for LD690 in methanol due to Bardeen *et al.*[43] which exhibits similar absorption and emission curves. Spectra of organic chromophores are poorly reproduced by dephasing models such as that used here, due to the extensive Lorentzian wings which result from assuming an unphysical delta correlated modulation process. Nonetheless, the Voigt lineshape introduced by Shank and co-workers for their simulation would in fact produce a $1/e$ dipole decay of $\sim$18 fs, close to the $\sim$13 fs used here. Considering the differences in the two lineshape functions, the agreement is even better. The simple model used has thus led to physically meaningful dephasing parameters, lending further confidence to this approach.

The only additional molecular characteristics used for the simulations were detunings which can be assessed directly from the spectra, as well as a reaction coordinate masquerading as a highly displaced vibrational mode. The latter is far too simplified to be directly compared with the intricate dephasing models proposed for B-30.[39] Suffice it to say that the dynamic broadening and Gaussian phase decay induced by the highly displaced mode closely resembles the B-30 absorption band. The assignment of detuning magnitudes deserves further comment. The molding of coherences on the ground state is completed within the period of irradiation by the pump—a period which is itself defined by the amount of chirp. Thus the resonance frequency is in a sense chirp-dependent. For the laser dyes, due to the limited Stokes shifting of emission, this effect can be ignored and the detuning determined from the peaks of absorption and pump spectra. The B-30 case is more difficult, since intermolecular relaxation energies are huge, and very rapid. Defining the detuning there may be ambiguous. However, due to the dominance of the reactive dephasing in this case, this mechanism is of secondary importance. In any case, demonstrating the detuning effects is all the more important since the sources capable of generating very short laser pulses such as those used here are not widely tunable, and as a result a certain amount of pump detuning is often unavoidable.

Since it is the sole system comprehensively studied before, it is interesting to compare the optimal chirp obtained in our O-1 experiments with that extracted by Malkmus *et al.* for this system solvated in methanol.[17] They report an optimal chirp of $\sim -60\ fs^2\ rad^{-1}$ for a 600 cm^{-1}, about 2 times larger than that obtained here. This is probably attributable to two factors, the smaller detuning employed there, and narrower bandwidth of their pump pulses. The former clearly produces a weaker effective dephasing, allowing for more extensive following. The latter is more involved, relating to the small widening factors for the OC pulses in both cases. Near the TL, the instantaneous chirp rate goes through a bandwidth dependent maximum, returning to zero at the TL. Deciding which of these factors is responsible to the change in OC must await experiments which systematically vary both.

A full discussion of dispersed-probe RISRS modulation phases and amplitudes is beyond the scope of this report, but has been covered in the literature.[10,12,25,35,37] Their λ-dependence involves interplay between dispersion and absorption whose simulation requires knowledge of all mode displacements and frequencies, as well as the excitation pulse spectrum. For the simpler case of solvent mode excitation, the results obtained match expectations as described.[2,3,12,13] Here, we emphasize the fact that these mappings are invariant with pump chirp, demonstrating the dominance of RISRS to the vibrational modulations observed. Since S_0 and S_1 coherences should exhibit distinct phase variations with wavelength, and vary in amplitude differently with chirp, contributions from both should lead to systematic alterations in the combined phase profiles for different pump GVD. This applies only for modes which vary negligibly in frequency upon photoexcitation, for otherwise the excited and ground states will contribute distinct Fourier components.

Consistency of the fitting parameters with the literature permits moving on to reconsider the research queries listed in the introduction, and to identify the lessons learned. First the crucial factors which influence chirp effects on IVS modulations in polyatomic chromophores have been identified, and their importance experimentally demonstrated. The simplest case of small displacement resonant excitation leading to mode-specific chirp contours is clearly demonstrated in S–B. Mode-interdependence is exhibited in its extreme in B-30 where a single highly displaced mode extinguishes long term chirp effects. Finally, detuning restrictions are clarified in O-1. In addition, all three systems show that at least to some degree,

NC will nearly always enhance ground state RISRS contributions to IVS, even in the presence of reactive or intermolecular dephasing effects. Accordingly, chirp can always be employed to differentiate multiple contributions to this observable, but to an extent dictated by molecular parameters.

A less well understood aspect of our results involves the lack of clear evidence for excited state contributions to the IVS signals. In B-30 this might reflect dispersive excited state dynamics due to an anharmonic reaction coordinate. But, this cannot explain their absence in the IVS of the two laser dyes examined as well, since both are textbook examples for mirror image relations between absorption and emission in fluorescent molecules,[44] and similar dyes were claimed to present a significant excited state activity in previous works. Our assignment is not based on frequencies, which can be similar in S_0 and S_1, but rather on the chirp invariance in the phase contours, along with the high quality fit provided by an exclusive RISRS model and the lack of frequency shifts with probing wavelength or with different chirps. Moreover, a sliding window Fourier transform (SWFT) analysis (not shown here) didn't demonstrate clear evolution of vibrational modes in time. Adding our results to the general difficulties of observing excited state modulations using IVS, the lack of excited state features in the laser dyes is important and intriguing. More work will be required to understand this absence of excited state signatures in the experiments.

Another point worthy of attention is the limitation of current work to linearly chirped pulses. Higher-order chirp terms are expected to have influence on coherences creation, but this wasn't studied before. Moreover, as non-linear optimal chirp for population transfer (minimization of excited state population) was recently shown to outperform the effects of the optimal linear one in an organic dye,[34,45] finding the analogue for maximizing RISRS signal is intriguing.

Finally, extensions of this approach could increase the depth of derived insights. When discussing the crude dephasing model employed in our analysis, mention was made of more elaborate approaches which are used to analyze molecular photophysics in condensed phases. Extracting the numerous parameters involved in such models requires not only measurement of absorption and resonance Raman line shapes, but determining absolute absorption and scattering cross sections.[46] In principle such cross sections should be obtainable from measurements of absolute amplitudes of spectral modulatons in impulsive spectra as well.[47] Despite the fact that this may be a simpler method for deriving absolute Raman cross sections, no such use has been reported. Once this dimension is added to the simulation, as well as an inclusion of the precise spectrum of pump and probe pulses, further details of medium effects should be revealed in IVS data as well.

F. Conclusions

Chirp effects on impulsively-induced vibrational wave packets have been investigated experimentally and theoretically. The objective was to identify the factors which influence these effects in large polyatomic chromophores in solution. A particular focus involved the definition of the optimal chirp for creating ground state coherences in a system with multiple displaced modes.

Comparison of ultrafast chirped pump—hyperspectral probe experiments with multi-mode simulations shows that the effects of GVD on the buildup of ground state wavepackets depend on the pulse spectrum, the displacements of vibrational modes, the detuning of the excitation pulses from resonance, and on electronic dephasing rates. Within the small-displacement regime, relevant for most laser dyes, each mode responds to excitation chirp independently, leading to mode-specific optimal chirp. Highly displaced modes entangle the dynamics of excitation in different modes, requiring a multi-dimensional description of the response.

Electronic dephasing and/or photo-reactivity narrow the window of opportunity for coherent manipulation, reducing the optimal chirp of all active modes. Our results show that selective enhancement of ground state vibrational coherences by NC is general, making this a viable tool for differentiating excited and ground state contributions to IVS. Moreover, for the three organic dyes studied, no obvious excited state contributions to the spectral modulations were discovered. Further study will be required to clarify this point. Finally, our non-intuitive results for low-Δ and slow dephasing regime regarding revivals of oscillation ever for large GVD's are still waiting for experimental demonstrations.

Acknowledgements

We thank E. Mastov for technical assistance. This work was partially supported by the US-Israel Binational Science Foundation (BSF). S.K. acknowledges the Sonderforschungsbereich 450 for a fellowship. The Farkas and Fritz-Haber research centers are supported by the Minerva Gesellschaft für die Forschung GmbH, München, Germany.

References

1 L. Dhar, J. A. Rogers and K. A. Nelson, *Chem. Rev.*, 1994, **94**(1), 157–193.
2 S. Ruhman, A. G. Joly and K. A. Nelson, *J. Chem. Phys.*, 1987, **86**(11), 6563–6565.
3 J. Chesnoy and A. Mokhtari, *Phys. Rev. A: At., Mol., Opt. Phys.*, 1988, **38**(7), 3566–3576.
4 B. Hartke, R. Kosloff and S. Ruhman, *Chem. Phys. Lett.*, 1989, **158**(3–4), 238–244.
5 U. Banin, A. Waldman and S. Ruhman, *J. Chem. Phys.*, 1992, **96**(3), 2416–2419; U. Banin and S. Ruhman, *J. Chem. Phys.*, 1993, **98**(6), 4391–4403; U. Banin, A. Bartana, S. Ruhman and R. Kosloff, *J. Chem. Phys.*, 1994, **101**(10), 8461–8481; E. Gershgoren, J. Vala, R. Kosloff and S. Ruhman, *J. Phys. Chem. A*, 2001, **105**(21), 5081–5095.
6 D. M. Jonas, S. E. Bradforth, S. A. Passino and G. R. Fleming, *J. Phys. Chem.*, 1995, **99**(9), 2594–2608.
7 G. Cerullo, L. Lüer, C. Manzoni, S. De-Silvestri, O. Shoshana and S. Ruhman, *J. Phys. Chem. A*, 2003, **107**(40), 8339–8344.
8 G. Cerullo and S. De-Silvestri, *Rev. Sci. Instrum.*, 2003, **74**(1), 1–18.
9 T. Kobayashi and A. Baltuska, *Meas. Sci. Technol.*, 2002, **13**(11), 1671–1682.
10 W. T. Pollard, H. L. Fragnito, J.-Y. Bigot, C. V. Shank and R. A. Mathies, *Chem. Phys. Lett.*, 1990, **168**(3–4), 239–245.
11 W. T. Pollard, S. L. Dexheimer, Q. Wang, L. A. Peteanu, C. V. Shank and R. A. Mathies, *J. Phys. Chem.*, 1992, **96**(15), 6147–6158.

12 A. T. N. Kumar, F. Rosca, A. Widom and P. M. Champion, *J. Chem. Phys.*, 2001, **114**(2), 701–724; A. T. N. Kumar, F. Rosca, A. Widom and P. M. Champion, *J. Chem. Phys.*, 2001, **114**(15), 6795–6815.
13 A. L. Dobryakov and N. P. Ernsting, *J. Chem. Phys.*, 2008, **129**(18), 184504.
14 S. Ruhman and R. Kosloff, *J. Opt. Soc. Am. B*, 1990, **7**(8), 1748–1752.
15 J. L. Krause, R. M. Whitnell, K. R. Wilson, Y.-J. Yan and S. Mukamel, *J. Chem. Phys.*, 1993, **99**(9), 6562–6578.
16 C. J. Bardeen, Q. Wang and C. V. Shank, *J. Phys. Chem. A*, 1998, **102**(17), 2759–2766; C. J. Bardeen, Q. Wang and C. V. Shank, *Phys. Rev. Lett.*, 1995, **75**(19), 3410–3413.
17 S. Malkmus, R. Durr, C. Sobotta, H. Pulvermacher, W. Zinth and M. Braun, *J. Phys. Chem. A*, 2005, **109**(46), 10488–10492; M. Braun, C. Sobotta, R. Durr, H. Pulvermacher and S. Malkmus, *J. Phys. Chem. A*, 2006, **110**(32), 9793–9800.
18 A. Kahan, O. Nahmias, N. Friedman, M. Sheves and S. Ruhman, *J. Am. Chem. Soc.*, 2007, **129**(3), 537–546.
19 M.-C. Yoon, J. K. Song, S. Cho and D. Kim, *Bull. Korean Chem. Soc.*, 2003, **24**(8), 1075–1080.
20 G. Lanzani, M. Zavelani-Rossi, G. Cerullo, D. Comoretto and G. Dellepiane, *Phys. Rev. B: Condens. Matter Mater. Phys.*, 2004, **69**(13), 134302.
21 To be exact, this study (ref. 17) reports on two dominant modes, but their frequency vicinity (560 cm^{-1} *vs.* 609 cm^{-1}) doesn't allow a real distinction between them. Moreover, interpretation was done following a one-dimensional scenario.
22 A. B. Myers, R. A. Mathies, D. J. Tannor and E. J. Heller, *J. Chem. Phys.*, 1982, **77**(8), 3857–3866.
23 R. Kosloff, *J. Phys. Chem.*, 1988, **92**(8), 2087–2100.
24 G. Lindblad, *Commun. Math. Phys.*, 1976, **48**(2), 119–130.
25 P. Nuernberger, *Opt. Commun.*, 2009, **282**(2), 227–235.
26 G. Ashkenazi, U. Banin, A. Bartana, R. Kosloff and S. Ruhman, in *Adv. Chem. Phys.*, ed. I. Prigogine and S. A. Rice, John Wiley & Sons, USA, 1997, vol. 100, pp. 229–315.
27 N. Dudovich, B. Dayan, S. M. G. Faeder and Y. Silberberg, *Phys. Rev. Lett.*, 2001, **86**(1), 47–50.
28 P. W. Brumer and M. Shapiro, *Principles of the Quantum Control of Molecular Processes*, Wiley-Interscience, Berlin, 2003; S. A. Rice and M. Zhao, *Optical Control of Molecular Dynamics*, John Wiley & Sons, New York, 2000.
29 J. Cao, C. J. Bardeen and K. R. Wilson, *Phys. Rev. Lett.*, 1998, **80**(7), 1406–1409.
30 A. B. Myers and R. A. Mathies, in *Biological Application of Raman Spectroscopy: Vol. 2—Resonance Raman Spectra of Polyenes and Aromatics*, ed. T. G. Spiro, John Wiley & Sons, New York, 1987, ch. 1, pp. 1–58.
31 O. Shoshanim and S. Ruhman, *J. Chem. Phys.*, 2008, **129**(4), 044502.
32 E. Zeek, K. Maginnis, S. Backus, U. Russek, M. M. Murnane, G. R. Mourou, H. Kapteyn and G. Vdovin, *Opt. Lett.*, 1999, **24**(7), 493–495.
33 E. Zeek, R. Bartels, M. M. Murnane, H. C. Kapteyn, S. Backus and G. Vdovin, *Opt. Lett.*, 2000, **25**(8), 587–589; R. Bartels, PhD Thesis, University of Michigan, 2002.
34 O. Nahmias, O. Bismuth, O. Shoshana and S. Ruhman, *J. Phys. Chem. A*, 2005, **109**(37), 8246–8253.
35 R. Trebino, K. W. DeLong, D. N. Fittinghoff, J. N. Sweetser, M. A. Krumbugel, B. A. Richman and D. J. Kane, *Rev. Sci. Instrum.*, 1997, **68**(9), 3277–3295.
36 L. Lüer, C. Gadermaier, J. Crochet, T. Hertel, D. Brida and G. Lanzani, *Phys. Rev. Lett.*, 2009, **102**(12), 127401.
37 RR data for S–B was not available—spectral parameters were compared with Oxazine-4 (LD690) in methanol having similar absorption and emission spectra (see ref. 43).
38 S. A. Kovalenko, N. Eilers-Konig, T. A. Senyushkina and N. P. Ernsting, *J. Phys. Chem. A*, 2001, **105**(20), 4834–4843.
39 X. H. Zhao, J. A. Burt and J. L. McHale, *J. Chem. Phys.*, 2004, **121**(22), 11195–11201.
40 S. Hogiu, J. Dreyer, M. Pfeiffer, K.-W. Brzezinka and W. Werncke, *J. Raman Spectrosc.*, 2000, **31**(8–9), 797–803.
41 H. Hwang and P. J. Rossky, *J. Phys. Chem. B*, 2004, **108**(21), 6723–6732.
42 G. R. Loppnow and R. A. Mathies, *Biophys. J.*, 1988, **54**(1), 35–43.
43 C. J. Bardeen, S. J. Rosenthal and C. V. Shank, *J. Phys. Chem. A*, 1999, **103**(49), 10506–10516.
44 (S–B) Exciton laser dyes database; (O-1): R. R. Birge, *Kodak Laser Dyes*, Kodak publication JJ-169, 1987; R. Sens and K. H. Drexhage, *J. Lumin.*, 1981, **24–25**, 709–712.
45 G. Cerullo, C. J. Bardeen, Q. Wang and C. V. Shank, *Chem. Phys. Lett.*, 1996, **262**(3–4), 362–368.
46 J. L. Mchale, *Acc. Chem. Res.*, 2001, **34**(4), 265–272.
47 Y.-X. Yan, E. B. Gamble and K. A. Nelson, *J. Chem. Phys.*, 1985, **83**(11), 5391–5399.